Title

Depiction of Achilles Tendon Microstructure In Vivo Using High-Resolution 3-Dimensional Ultrashort Echo-Time Magnetic Resonance Imaging at 7 T

Journal

Investigative Radiology, 49(5)

ISSN

0020-9996

Authors

Han, Misung
Larson, Peder EZ
Liu, Jing
et al.

Publication Date

2014-05-01

DOI

10.1097/rli.0000000000000025

Peer reviewed

Published in final edited form as:
Invest Radiol. 2014 May ; 49(5): 339–345. doi:10.1097/RLI.0000000000000025.

Depiction of Achilles Tendon Microstructure In-Vivo Using High-Resolution 3D Ultrashort Echo-Time MRI at 7T

Misung Han, PhD[1], **Peder E. Z. Larson, PhD**[1], **Jing Liu, PhD**[1], and **Roland Krug, PhD**[1]

[1]Department of Radiology and Biomedical Imaging, University of California, San Francisco, San Francisco, California, USA

Abstract

Objectives—To demonstrate the feasibility of depicting the internal structure of the Achilles tendon in vivo using high-resolution 3D ultrashort echo-time (UTE) magnetic resonance imaging (MRI) at 7T.

Materials and Methods—For our UTE imaging, a minimum-phase radiofrequency pulse and an anisotropic field-of-view 3D radial acquisition were used to minimize the echo time and scan time. A fat saturation pulse was applied every eight spoke acquisitions to reduce blurring and chemical shift artifacts from fat and to improve dynamic range of the tendon signal. Five healthy volunteers and one patient were scanned with an isotropic spatial resolution of up to 0.6 mm. Fat-suppressed UTE images were qualitatively evaluated and compared to non-fat-suppressed UTE images and longer echo-time images.

Results—High-resolution UTE imaging was able to visualize the microstructure of the Achilles tendon. Fat suppression substantially improved the depiction of the internal structure. The UTE images revealed a fascicular pattern in the Achilles tendon and fibrocartilage at the tendon insertion. In a patient who had tendon elongation surgery after birth there was clear depiction of disrupted tendon structure.

Conclusions—High-resolution fat-suppressed 3D UTE imaging at 7T allows for evaluation of the Achilles tendon microstructure in vivo.

Keywords

Achilles tendon; ultrashort echo-time MRI; tendon microstructure; ultra high field MRI; tendon fiber structure

Introduction

The Achilles tendon is the largest and strongest tendon in the human body, with 15 cm in length and 6 mm in thickness on average [1]. By connecting the calf muscles to the calcaneous bone, the Achilles tendon transmits the power of the calf muscles to the foot, facilitating running and jumping. To provide great strength during these locomotive

Correspondence to: Misung Han, PhD, China Basin Landing, 185 Berry Street, Suite 350, Box 0946, San Francisco, CA 94107, Fax: (415) 353-9423, Phone: (415) 353-4898, misung.han@ucsf.edu.

activities, the Achilles tendon possesses a highly ordered ultrastructure, being primarily composed of an array of collagen bundles (fascicles, secondary fiber bundles) separated by thin connective tissue (endotenon) [2]. The endotenon carries small vessels, lymphatics, and nerves.

Despite its strength, the Achilles tendon is one of the most frequently injured tendons with various types of traumatic and overuse conditions [3, 4]. Achilles tendon injuries range from inflammation of the paratendinous tissue (peritendinitis) and structural degeneration of the tendon (tendinosis) to partial or complete tendon rupture [4, 5]. Due to a higher participation in sports and recreation activities in modern societies, the incidence of Achilles tendon injuries is increasing [6, 7]. Thus, there is a high demand for accurate diagnosis and treatment of Achilles tendon injuries.

Currently, the imaging modalities that are most helpful for delineating tendon abnormalities are ultrasound and magnetic resonance imaging (MRI). Ultrasound is quick, relatively inexpensive, and non-invasive; allows for dynamic examination; and provides a higher spatial resolution than MRI (< 0.2 mm). With ultrasound, the tendon is represented with a fibrillar pattern of parallel hyperechoic lines in the longitudinal plane, caused by reflections at the boundaries of collagen bundles and endotenon [8]. A range of Achilles tendon abnormalities can be detected as hypoechoic regions [9, 10]. The major limitation of ultrasound is that the results are operator-dependent and it cannot differentiate partial ruptures from focal degenerative lesions [11]. MRI is more expensive and lacks the capability of dynamic imaging, but it is highly sensitive to pathological changes within the Achilles tendon [12, 13]. For most standard MR images, the healthy Achilles tendon is normally dark due to its very short T_2* relaxation time on the order of 1 ms and long T_1 relaxation time [14-16]. Therefore, evaluating tendon abnormalities has been based on detecting areas of increased signal within the tendon and assessing morphologic changes in the surrounding tissues. However, there are pitfalls because the healthy tendon can also generate high signal, which can be misinterpreted as tendon abnormalities. Connective tissue having a longer T_2* relaxation time than fascicles can generate increased signal-intensity stripes on sagittal images and punctuated foci on axial images [17-19]. When the tendon fiber is at an approximately 55° angle relative to the static magnetic field direction, a bright signal can be also seen in the distal end of the tendon due to magic angle effects [20].

Ultrashort echo-time (UTE) imaging uses specific radiofrequency (RF) pulses and acquisition methods to shorten the echo time (TE), allowing for a direct visualization of short T_2* components [14, 21, 22]. Recently, several studies have been performed to discriminate healthy tendons and pathological tendons using UTE imaging combined with contrast injection [15, 23], T_2* relaxation time quantification [15, 24], or magnetization transfer effect quantification [25, 26]. It was also shown that fiber structure can be delineated with high-resolution UTE imaging because of T_2* relaxation time difference between fascicles and endotenon [15, 27]. However, this fiber structure depiction has been shown only for ex-vivo specimens and limited regions of the in vivo Achilles tendon.

There is an increasing interest in using ultra high-field (7T) systems for musculoskeletal MRI [28, 29] mainly due to inherent increase in signal-to-noise ratio (SNR), which is

proportional to the field strength. However, ultra high-field MRI is challenging because of increased B_0 and B_1 inhomogeneities, limited availability of phased-array coils, and increased RF power deposition. Despite these challenges, the SNR improvement and better delineation of structural information at 7T over 3T has been demonstrated in many joints such as the knee [28-30] and ankle [31]. Several studies have shown that UTE imaging at 7T is also feasible, providing high signal from ultra-short T_2 components without substantial degradations in image quality [24, 32].

In this work, we used three-dimensional (3D) UTE imaging [33, 34] at 7T to demonstrate the feasibility of visualizing internal tendon microstructure in-vivo. The 3D UTE imaging can provide high isotropic resolution, which is helpful for evaluating complex structure. We optimized the 3D UTE sequence for the highest possible spatial resolution to depict the Achilles tendon and tested the pulse sequence on five healthy volunteers and one patient.

Materials and Methods

UTE Imaging Pulse Sequence

Our 3D UTE imaging sequence was developed for a MR950 7T scanner (GE Healthcare, Waukesha, WI, USA) equipped with a maximum gradient amplitude of 5 G/cm and maximum slew rate of 200 mT/m/ms. To achieve an ultrashort TE, a minimum-phase RF pulse was followed by 3D radial acquisition as shown in Fig. 1. The minimum-phase RF pulse was used instead of a non-selective hard pulse to limit the slab-direction field of view (FOV). A short RF pulse with a duration of 432 μs and a time-bandwidth product of three was used to minimize T_2* decay during excitation. This RF pulse was first designed using the Shinnar-Le Roux algorithm [35], and then the RF waveform was reshaped using the variable-rate selective excitation algorithm [36] to be played on the slab-select gradient ramps. The slab-selection rephasing gradient lobe was located following the slab-select gradient lobe.

For 3D radial imaging, *k*-space was traversed from the center to the periphery, starting data acquisition with the rising slope of the readout gradient (ramp sampling). The radial trajectories were determined based on the prescribed spatial resolution and FOV. In particular, an anisotropic FOV was supported with our radial trajectories, which can be tailored to a non-circular object instead of an isotropic FOV to reduce scan time [37]. The gradient delay for each axis was measured from the scanner and the sequence was adjusted to reduce the mismatch between the actual and ideal trajectories. Readout gradients were fully rewound after data acquisition and a gradient spoiler was added along the *z* direction.

Fat suppression was performed to improve dynamic range of tendon signal and remove any blurring and chemical shift artifacts [38] from fat. The fat saturation pulse used was a minimum-phase pulse with a 90° flip angle, 1 kHz bandwidth, and 4 ms pulse duration. The center frequency of this pulse was -1043 Hz below the water resonant frequency, and it was applied every eight spoke acquisitions to minimally increase the scan time.

In Vivo Experiments

Five healthy volunteers (under age 35) and one patient (age 32) operated with a tendon elongation surgery (splitting the tendon and then sewing together) right after birth were imaged at 7T. Informed consent was obtained prior to scans. A head-only quadrature coil was used to transmit and a 32-channel phased-array head coil (Nova Medical, Wilmington, MA) was used to receive signal. The subjects laid supine with one foot located in the head coil. To fit the foot, the upper part of the phased-array coil was shifted off from its original location for head imaging. The leg was positioned as parallel to the B_0 field as possible to minimize magic angle effects.

For each subject, standard sagittal T_1-weighted 2D fast-spin echo (FSE) imaging and fat-suppressed T_2-weighted 2D FSE imaging were first performed, using 15 × 15 cm^2 FOV, 416 × 256 matrix size, 0.36 × 0.59 mm^2 spatial resolution, 21 slices, 3 mm slice thickness, and ±41.7 kHz readout bandwidth. As other scan parameters, T_1-weighted FSE used a repetition time (TR) of 764 ms, TE of 8.6 ms, echo train length of 3, and averaging of 2, while fat-suppressed T_2-weighted FSE used a TR of 3407 ms, TE of 68.8 ms, echo train length of 8, and averaging of 3. The total scan time was 4 min for T_1-weighted FSE and 5 min for fat-suppressed T_2-weighted FSE. High-resolution UTE imaging with TR/TE = 8 ms/229 μs was performed with applying slab-selection along the superior to inferior direction. The flip angle was optimized to 8° assuming T_1 of tendon was 800 ms [16, 39]. The readout bandwidth was ±250 kHz, the readout time was 0.768 ms, and either 0.6 mm or 0.65 mm isotropic spatial resolution was used with prescribing a FOV of 15 × 9 × 12.2 cm^3 or 14 × 8.4 × 11.6 cm^3 respectively. This resulted in the number of spokes to acquire as 110797 or 114816 and the scan time as approximately 18 min. For some of the healthy volunteers, longer-echo images (with TE of 2.2 ms) or UTE images without fat suppression were additionally acquired.

UTE image reconstruction was performed off-line with 3D gridding using a Kaiser-Bessel kernel [40] followed by an inverse Fourier transform. The acquired data from the 16 coil elements located on the anterior part of the head coil were not used for reconstruction. The coil images from the remaining 16 elements were combined using a sum of squares. UTE images with and without fat suppression as well as UTE images with longer-TE images were qualitatively compared.

Results

For all subjects, high-resolution UTE imaging was able to visualize the Achilles tendon directly and depict its internal microstructure. Figure 2 demonstrates results from one healthy volunteer. Figure 2a-b shows sagittal reformatted slices from fat-suppressed 3D UTE imaging with two different TEs of 229 μs and 2.2 ms. An isotropic spatial resolution of 0.65 mm was used. With a TE of 229 μs, the tendon had relatively high signal depicting the fascicular pattern, where stripes of higher signal represented endotenon while those of lower signal represented fascicles. A high signal was also observed at the tendon insertion to the calcaneous bone (enthesis, dashed arrow), which consists of fibrocartilage. The structure, histology, and MR imaging of the enthesis are well presented in these articles [15, 41, 42]. With a TE of 2.2 ms, the tendon became mostly dark; however, some of the bright strips that

were present in Fig. 2a and the enthesis were still visible, indicating that T_2* relaxation times in those regions were higher than in other regions of the tendon. A standard T_1-weighted FSE image and a standard fat-suppressed T_2-weighted FSE image at the matching position are shown in Fig. 2c-d. In Fig. 2c, bright strips were observed at the locations close to those at Fig. 2b (solid arrow); in Fig. 2d, they were almost non-existent.

UTE images with and without fat suppression acquired from a different healthy volunteer are compared in Fig. 3. An isotropic resolution of 0.6 mm was used. Figure 3 clearly demonstrates that fat suppression improved the conspicuity of the Achilles tendon by reducing blurring and chemical shift artifacts from the fat. Without fat suppression, a bright signal was generated at the boundary of the tendon adjacent to Kager's triangle (depicted by a solid arrow) and the internal tendon structure was less pronounced. The signal from the tendon was partially saturated by the fat suppression pulse because the tendon has a short T_2* value and therefore has a wide spectrum. Based on regions-of-interest analysis, fat suppression decreased the tendon signal by 23%.

Figure 4 shows axial reformatted slices from fat-suppressed UTE images of the volunteer as in Fig. 3. Slices at six different positions along the inferior to superior direction (positions denoted in (a)), including the insertion site (b-c), proximal to the insertion site (d), and the musculotendinous junction (g), are presented here. In (b), the enthesis fibrocartilage was visible as a bright signal (solid arrow). This cartilage was visible in (c) again, and additionally the sesamoid fibrocartilage (dashed arrow) and a fascicular pattern in the posterior part of the tendon were depicted. At superior levels above the insertion site, the fibrocartilage was not detected and a fascicular pattern was demonstrated over the entire tendon.

The ability to assess the tendon structure in arbitrary planes with our high-resolution isotropic UTE imaging is demonstrated again in Fig. 5. Here, an axial, sagittal, and coronal reformatted slice from fat-suppressed UTE images of the equivalent ankle as in Fig. 2a are shown. A fascicular pattern was shown in each slice and in particular the directions of groups of fascicles were discernible in the coronal reformatted slice. Three different groups of fascicles were distinguishable (denoted by solid arrows), varying in where they originated from and which part of the calcaneous bone they were attached to.

Images from a 32 year-old patient who had tendon elongation surgery right after birth are shown in Fig. 6. Sagittal reformatted slices from UTE imaging at the locations denoted in Fig. 6a and T_1-weighted 2D FSE images at the matching locations are presented. On the FSE images, bright signal was generated due to fat infiltration (solid arrows), but destruction on the tendon fiber structure was not clear. However, UTE images were able to depict disrupted fiber microstructure and discontinuous fascicles in the region of the former tendon incision.

Discussion

In this work, we have presented the feasibility of an optimized high-resolution 3D UTE imaging for the depiction of the Achilles tendon microstructure on a 7T clinical scanner. No

hardware modifications were required with our technique. The Achilles tendon generated relatively high signal that revealed a fascicular pattern, differentiating fascicles and endotenon due to their different T_2* relaxation times. The enthesis, being commonly involved in overuse injuries in sport [5, 43], was well delineated as well. The 3D isotropic imaging allowed for evaluating tendon microstructures in arbitrary planes, which was useful in assessing these complex structures.

Ignoring relaxation effects, SNR increases with the field strength due to increased magnetization; however, this theoretical SNR increase is not normally realized in vivo due to increase in T_1 and decrease in T_2*. We measured T_2* in the mid-region of the Achilles tendon by acquiring images at six TEs (0.25, 0.5, 1, 2, 4, and 8 ms at 3T; 0.23, 0.5, 1, 2, 3, and 5 ms at 7T) for one volunteer at both 3T and 7T. The estimated T_2* was 1.2 ms at 3T and 0.85 ms at 7T. Even with T_2* decrease at 7T, the effect on the signal is only a 9% decrease when using an ultrashort TE of 230 μs. The overall SNR gain at 7T over 3T in the Achilles tendon is expected to be 114% with our UTE imaging if T_1 difference is ignored. In our work, the excitation flip angle was only optimized to provide the highest SNR from the tendon not considering contrast-to-noise ratios with surrounding tissues. However, the tendon was differentiated because adjacent Kager's triangle and bone marrow were suppressed with fat saturation and muscle as well as skin provided higher signal than the Achilles tendon. On UTE images, adjacent muscle generated 66% and 36% higher signal than the tendon at 3T and 7T, respectively. Increased B_0 and B_1 inhomogeneities, increased RF power deposition, and lack of dedicated phased-array coils are challenges for 7T MRI. However, using a low flip angle (8°) made our UTE imaging to be minimally sensitive to B_0 and B_1 inhomogeneities and generated low RF power deposition. The head array coil was sufficient for all subjects and provided high SNR on the Achilles tendon.

Fat suppression is very important for this application because large off-resonances from fat (> 1 kHz) can cause blurring and chemical shift artifacts with 3D radial acquisitions. These artifacts can affect the structural analysis of the surrounding tissues. We observed that when fat suppression was not applied, artifacts from the adjacent Kager's triangle degraded the depiction of the tendon microstructure. As a fat suppression method, we used spectrally selective saturation. This method is normally sensitive to B_0 and B_1 inhomogeneities, but the larger resonant frequency difference between fat and water at 7T than at a lower field strengths results in reduced saturation of the broad short T_2 component and allows for design of a shorter saturation pulse that is less sensitive to B_0 and T_2. Alternatively, a short inversion time inversion recovery (STIR) technique can be used. This method is less sensitive to B_0 inhomogeneities and can be also insensitive to B_1 inhomogeneities when an adiabatic inversion pulse is used. However, a longer scan time is typically required due to the inversion time, which is challenging with a large number of spokes required in 3D UTE imaging.

The readout time substantially affects image quality for UTE imaging. When it is longer, more blurring artifacts are caused by off-resonances and the signal decay of ultra-short T_2* components [34]. To minimize these artifacts, the readout time should be as short as possible while providing a proper gradient area and satisfying the maximum amplitude and slew rate constraints. It was demonstrated that the optimized readout time for 3D UTE

imaging is 0.69 T_2* [34], which provides the maximum SNR while generating minimal blurring artifacts for ultra-short T_2* components. The readout time we used was 0.77 ms, which was longer than the optimal value 0.59 ms given that T_2* of the tendon was 0.85 ms. Reducing the readout time would further improve the depiction of the Achilles tendon structure.

Radial trajectories are commonly used to minimize the TE but this is more vulnerable to image artifacts caused by system imperfections than conventional Cartesian trajectories. In particular, eddy currents and group delays of gradient amplifiers result in mismatches between the prescribed and actual trajectories and degrade image quality [44]. In this work, we corrected for gradient delays, which improved image quality significantly. More advanced techniques such as measuring the actual trajectories [45] can also be incorporated to further correct for system imperfections. Because 3D radial acquisitions are not very sensitive to motion [46], no visible motion artifacts were seen even with 18 minute scan time. This scan time can be easily reduced in future studies by combining with parallel imaging.

We have demonstrated that our optimized high-resolution 3D UTE sequence can visualize internal fiber structures down to the level of the fascicle. Since the diameter of the fascicle in human is known to be in a range of 150 μm - 1 mm [47], it is reasonable that our UTE imaging depicts fascicular patterns. Our patient images clearly depicted disrupted tendon microstructure due to the incision from the tendon elongation surgery. Ultrasound also provides internal structure of the tendon down to this level, but MRI might be more useful because of the capability to assess pathologies in surrounding organs including bone marrow and Kager's triangle. Future work will include patient studies to demonstrate the feasibility of 3D UTE imaging to depict changes in the fiber structure with early degeneration, to monitor the healing process after rupture, and to evaluate different treatment options.

In conclusion, our 3D UTE pulse sequence allows for high-resolution structural imaging of the Achilles tendon in vivo using a clinical 7T MRI scanner without specialized hardware. The combination of a minimum-phase slab-selective RF pulse and anisotropic FOV 3D radial trajectory provided a high-resolution UTE imaging of the Achilles tendon within a clinically feasible scan time, and fat suppression greatly improved the depiction of the tendon microstructure. Our approach demonstrated a normal fascicular pattern in the healthy Achilles tendon with differentiating fascicles and endotenon and delineated fibrocartilage at the tendon insertion. Disrupted tendon microstructure was also visualized on patient images.

Acknowledgments

Grant Sponsors: This work was supported by NIH R01AR057336, S10 RR026845, and UCSF Radiology Seed Grant.

References

1. Schweitzer ME, Karasick D. MR imaging of disorders of the Achilles tendon. Am J Roentgenol. 2000; 175:613–625. [PubMed: 10954440]
2. Elliott DH. Structure and function of mammalian tendon. Biol Rev. 1965; 40:392–421. [PubMed: 14340913]

3. Leppilahti J, Orava S, Karpakka J, et al. Overuse injuries of the Achilles tendon. Ann Chir Gynaecol. 1991; 80:202–207. [PubMed: 1897887]
4. Galloway MT, Jokl P, Dayton OW. Achilles tendon overuse injuries. Clin Sports Med. 1992; 11:771–782. [PubMed: 1423697]
5. Kvist M. Achilles tendon injuries in athletes. Sports Med. 1994; 18:173–201. [PubMed: 7809555]
6. Möller A, Aström M, Westlin NE. Increasing incidence of Achilles tendon rupture. Acta Orthop Scand. 1996; 67:479–481. [PubMed: 8948254]
7. Leppilahti J, Puranen J, Orava S. Incidence of Achilles tendon rupture. Acta Orthop Scand. 1996; 67:277–279. [PubMed: 8686468]
8. Martinoli C, Derchi LE, Pastorino C, et al. Analysis of echotexture of tendons with US. Radiology. 1993; 186:839–843. [PubMed: 8430196]
9. Martinoli C, Bianchi S, Derchi LE. Tendon and nerve sonography. Radiol Clin North Am. 1999; 37:691–711. [PubMed: 10442076]
10. Grassi W, Filippucci E, Farina A, et al. Sonographic imaging of tendons. Arthritis Rheum. 2000; 43:969–976. [PubMed: 10817548]
11. Paavola M, Paakkala T, Kannus P, et al. Ultrasonography in the differential diagnosis of Achilles tendon injuries and related disorders. A comparison between pre-operative ultrasonography and surgical findings. Acta Radiol. 1998; 39:612–9. [PubMed: 9817030]
12. Marcus DS, Reicher MA, Kellerhouse LE. Achilles tendon injuries: the role of MR imaging. J Comput Assist Tomogr. 1989; 13:480–486. [PubMed: 2723180]
13. Aström M, Gentz C, Nilsson P, et al. Imaging in chronic achilles tendinopathy: a comparison of ultrasonography, magnetic resonance imaging and surgical findings in 27 histologically verified cases. Skeletal Radiol. 1996; 25:615–620. [PubMed: 8915043]
14. Gold GE, Pauly JM, Macovski A, et al. MR spectroscopic imaging of collagen: tendons and knee menisci. Magn Reson Med. 1995; 34:647–654. [PubMed: 8544684]
15. Robson MD, Benjamin M, Gishen P, et al. Magnetic resonance imaging of the Achilles tendon using ultrashort TE (UTE) pulse sequences. Clin Radiol. 2004; 59:727–735. [PubMed: 15262548]
16. Filho GH, Du J, Pak BC, et al. Quantitative characterization of the Achilles tendon in cadaveric specimens: T1 and T2* measurements using ultrashort-TE MRI at 3 T. Am J Roentgenol. 2009; 192:117–124. [PubMed: 19098189]
17. Rollandi G, Bertolotto M, Perrone R, et al. MRI of normal Achilles tendon. Eur Radiol. 1995; 5:596–598.
18. Mantel D, Flautre B, Bastian D, et al. Structural MRI study of the Achilles tendon. Correlation with microanatomy and histology. J Radiol. 1996; 77:261–265. [PubMed: 8734206]
19. Soila K, Karjalainen PT, Aronen HJ, et al. High-resolution MR imaging of the asymptomatic Achilles tendon: new observations. Am J Roentgenol. 1999; 173:323–328. [PubMed: 10430128]
20. Erickson SJ, Cox IH, Hyde JS, et al. Effect of tendon orientation on MR imaging signal intensity: a manifestation of the “magic angle” phenomenon. Radiology. 1991; 181:389–392. [PubMed: 1924777]
21. Robson MD, Gatehouse PD, Bydder M, et al. Magnetic resonance: an introduction to ultrashort TE (UTE) imaging. J Comput Assist Tomogr. 2003; 27:825–46. [PubMed: 14600447]
22. Gatehouse PD, Bydder GM. Magnetic resonance imaging of short T2 components in tissue. Clin Radiol. 2003; 58:1–19. [PubMed: 12565203]
23. Hodgson RJ, Grainger AJ, O’Connor PJ, et al. Imaging of the Achilles tendon in spondyloarthritis: a comparison of ultrasound and conventional, short and ultrashort echo time MRI with and without intravenous contrast. Eur Radiol. 2011; 21:1144–52. [PubMed: 21190022]
24. Juras V, Zbyn S, Pressl C, et al. Regional variations of T2* in healthy and pathologic achilles tendon in vivo at 7 Tesla: preliminary results. Magn Reson Med. 2012; 68:1607–1613. [PubMed: 22851221]
25. Hodgson RJ, Evans R, Wright P, et al. Quantitative magnetization transfer ultrashort echo time imaging of the achilles tendon. Magn Reson Med. 2011; 65:1372–1376. [PubMed: 21500263]

26. Grosse U, Syha R, Martirosian P, et al. Ultrashort echo time MR imaging with off-resonance saturation for characterization of pathologically altered Achilles tendons at 3 T. Magn Reson Med. 2013; 70:184–192. [PubMed: 22851408]
27. Koblik PD, Freeman DM. Short echo time magnetic resonance imaging of tendon. Invest Radiol. 1993; 28:1095–1100. [PubMed: 8307712]
28. Regatte RR, Schweitzer ME. Ultra-high-field MRI of the musculoskeletal system at 7.0T. J Magn Reson Imaging. 2007; 25:262–9. [PubMed: 17260399]
29. Krug R, Stehling C, Kelley DAC, et al. Imaging of the musculoskeletal system in vivo using ultra-high field magnetic resonance at 7 T. Invest Radiol. 2009; 44:613–618. [PubMed: 19652609]
30. Welsch GH, Juras V, Szomolanyi P, et al. Magnetic resonance imaging of the knee at 3 and 7 Tesla: a comparison using dedicated multi-channel coils and optimised 2D and 3D protocols. Eur Radiol. 2012; 22:1852–1859. [PubMed: 22538628]
31. Juras V, Welsch G, Bar P, et al. Comparison of 3T and 7T MRI clinical sequences for ankle imaging. Eur J Radiol. 2011; 81:1846–1850. [PubMed: 21665397]
32. Krug R, Larson PEZ, Wang C, et al. Ultrashort echo time MRI of cortical bone at 7 tesla field strength: a feasibility study. J Magn Reson Imaging. 2011; 34:691–695. [PubMed: 21769960]
33. Glover GH, Pauly JM, Bradshaw KM. Boron-11 imaging with a three-dimensional reconstruction method. J Magn Reson Imaging. 1992; 2:47–52. [PubMed: 1623280]
34. Rahmer J, Bornert P, Groen J, et al. Three-dimensional radial ultrashort echo-time imaging with T2 adapted sampling. Magn Reson Med. 2006; 55:1075–1082. [PubMed: 16538604]
35. Pauly J, Le Roux P, Nishimura D, et al. Parameter relations for the Shinnar-Le Roux selective excitation pulse design algorithm [NMR imaging]. IEEE Trans Med Imaging. 1991; 10:53–65. [PubMed: 18222800]
36. Conolly SM, Nishimura D, Macovski A, et al. Variable-rate selective excitation. J Magn Reson. 1988; 78:440–458.
37. Larson PZ, Gurney PT, Nishimura DG. Anisotropic field-of-views in radial imaging. IEEE Trans Med Imaging. 2008; 27:47–57. [PubMed: 18270061]
38. Bydder GM, Chung CB. Magnetic resonance imaging of short T2 relaxation components in the musculoskeletal system. Skeletal Radiol. 2009; 38:201–205. [PubMed: 18941741]
39. Wright P, Jellus V, McGonagle D, et al. Comparison of two ultrashort echo time sequences for the quantification of T1 within phantom and human Achilles tendon at 3 T. Magn Reson Med. 2012; 68:1279–1284. [PubMed: 22246857]
40. Beatty PJ, Nishimura DG, Pauly JM. Rapid gridding reconstruction with a minimal oversampling ratio. IEEE Trans Med Imaging. 2005; 24:799–808. [PubMed: 15959939]
41. Rufai A, Ralphs JR, Benjamin M. Structure and histopathology of the insertional region of the human Achilles tendon. J Orthop Res. 1995; 13:585–593. [PubMed: 7674075]
42. Benjamin M, Bydder GM. Magnetic resonance imaging of entheses using ultrashort TE (UTE) pulse sequences. J Magn Reson Imaging. 2007; 25:381–389. [PubMed: 17260402]
43. Benjamin M, Toumi H, Ralphs JR, et al. Where tendons and ligaments meet bone: attachment sites (‘entheses’) in relation to exercise and/or mechanical load. J Anat. 2006; 208:471–490. [PubMed: 16637873]
44. Peters DC, Derbyshire JA, McVeigh ER. Centering the projection reconstruction trajectory: reducing gradient delay errors. Magn Reson Med. 2003; 50:1–6. [PubMed: 12815671]
45. Duyn JH, Yang Y, Frank JA, et al. Simple Correction Method for k-Space Trajectory Deviations in MRI. J Magn Reson. 1998; 132:150–153. [PubMed: 9615415]
46. Glover GH, Pauly JM. Projection reconstruction techniques for reduction of motion effects in MRI. Magn Reson Med. 1992; 28:275–289. [PubMed: 1461126]
47. Kannus P. Structure of the tendon connective tissue. Scand J Med Sci Sports. 2000; 10:312–320. [PubMed: 11085557]

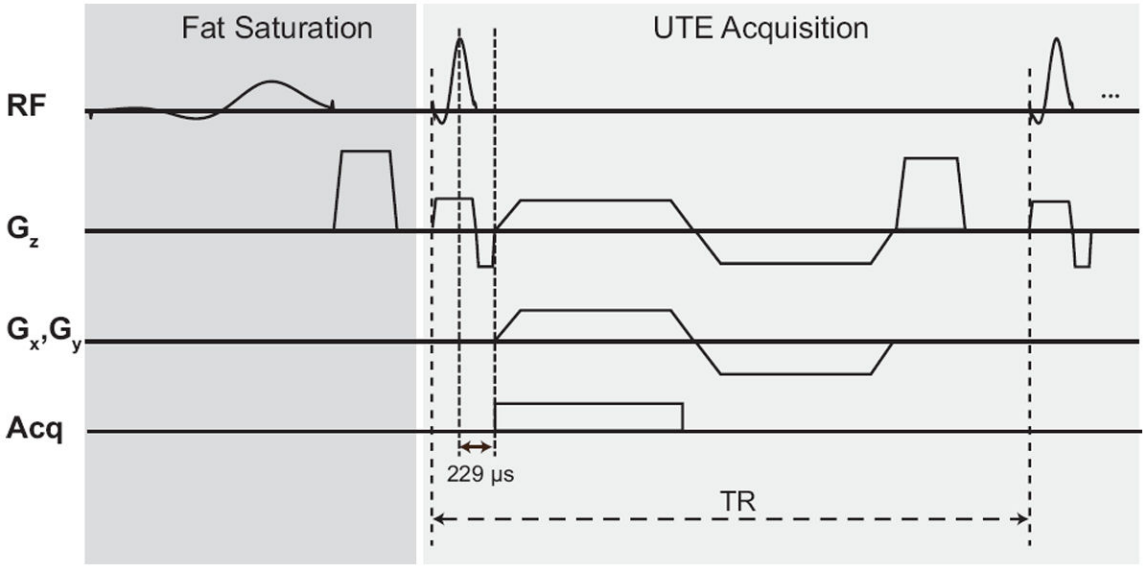

Figure 1.

Pulse sequence for 3D UTE imaging. By using a short minimum-phase RF pulse and 3D radial trajectory, a TE of 229 μs was achieved when the slab was 12 cm thick. A fat suppression pulse was applied every eight spoke acquisitions.

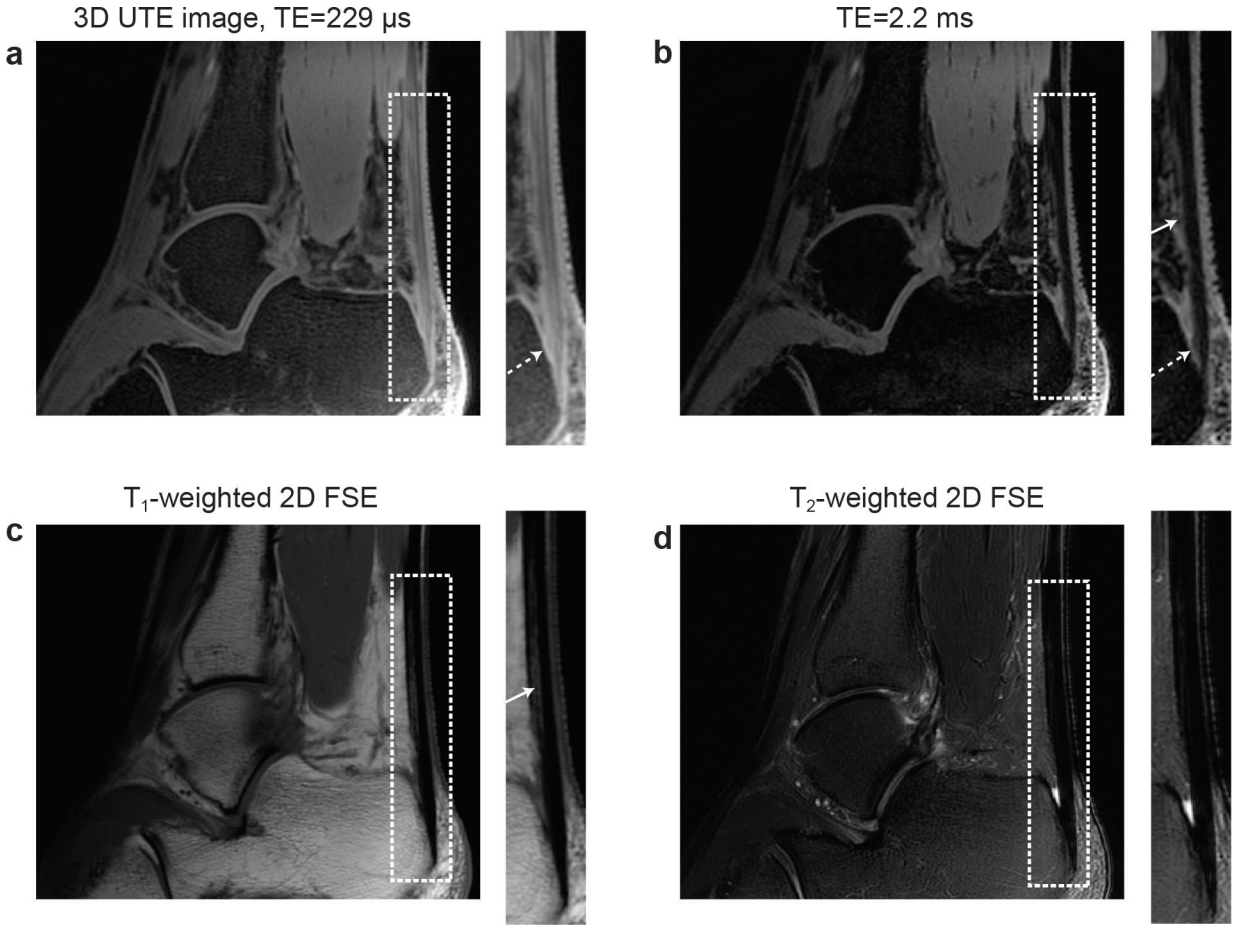

Figure 2.

UTE images and standard FSE images from a healthy volunteer. Magnified images of the tendon are shown on the right. (a-b) Sagittally-reformatted slices from fat-suppressed 3D UTE sequence, having TEs of 229 μs and 2.2 ms. In (a), a fascicular pattern is depicted in the tendon. In addition, high signal is observed at the enthesis (tendon insertion), which is consisted of fibrocartilage (dashed arrow). In (b), the tendon is much darker but some of the bright strips shown in (a) (solid arrow) and the enthesis are still visible. (c-d) Matching slices from standard T_1-weighted FSE and fat-suppressed T_2-weighted FSE. In both FSE images, the tendon generates almost no signal but the bright strips at the similar locations in (b) are visible in (c) (solid arrow). Here, the slice thickness for the UTE images is 0.65 mm while this for the FSE images is 3 mm.

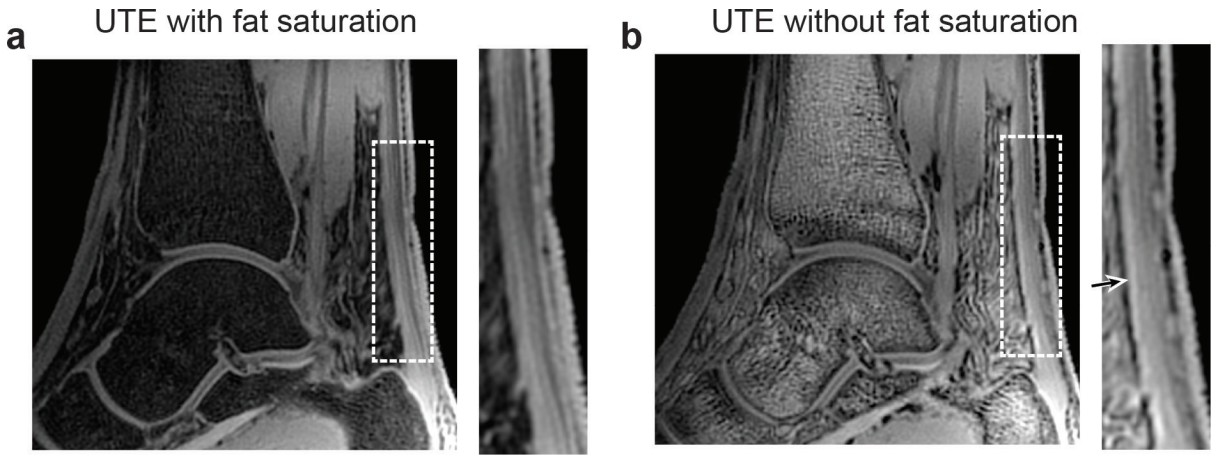

Figure 3.

Comparison of UTE images with and without fat suppression. Sagittal reformatted slices from 3D UTE imaging with (a) and without (b) fat suppression. Magnified images of the tendon are shown on the right. With fat suppression, blurring and chemical shift artifacts from the fatty tissue are substantially reduced, improving the depiction of tendon microstructure. When fat suppression is not applied, a bright signal occurs at the boundary of the tendon adjacent to Kager's triangle (arrow) due to chemical shift artifacts from fat.

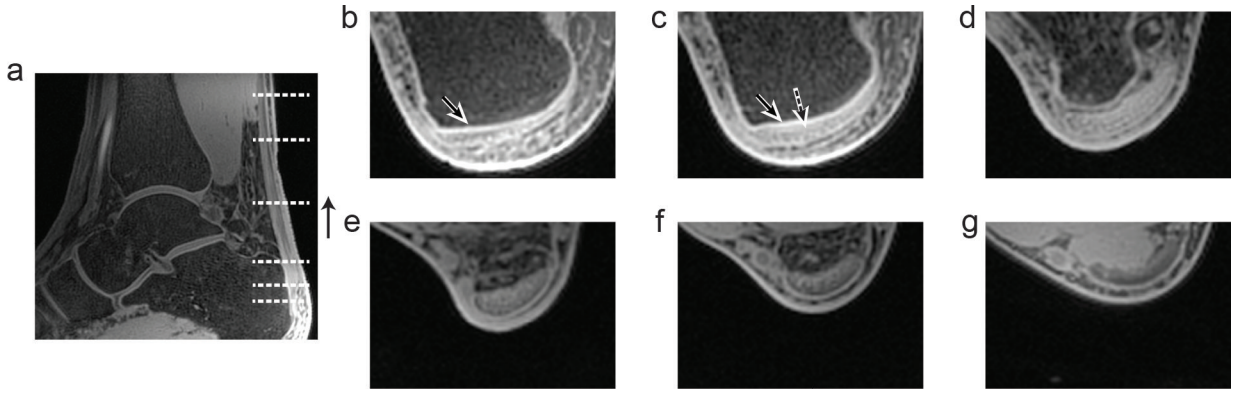

Figure 4.

Axial reformatted UTE slices at different locations along the Achilles tendon. On the sagittal reformatted UTE slice (a), the positions of six axial reformatted slices are denoted. In (b-g), the slices from the inferior to superior locations are shown. At the insertion site (b-c), the enthesis fibrocartilage is depicted as a bright signal (solid arrow). In (c), the sesamoid cartilage is also visible (dashed arrow) and a fascicular pattern is demonstrated in the posterior region of the tendon. At more superior levels, the fascicular pattern is visible throughout the whole Achilles tendon. The tendon is merged to the muscle at the musculotendinous junction (g).

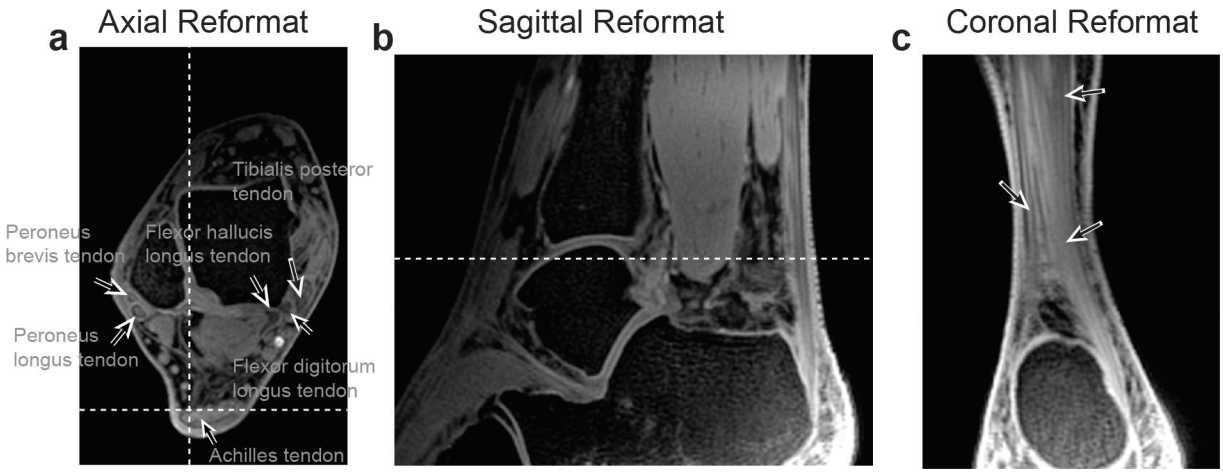

Figure 5.

Internal structural analysis of the Achilles tendon. (a-c) Axial, sagittal, and coronal reformatted slices. The positions of the slices are denoted as dashed lines in (a-b). A fascicular pattern is observed in the tendon. In (c), the orientations of the fascicles can be characterized, allowing for distinguishing different groups of fascicles as denoted by solid arrows. Numerous other tendons in the ankle are also well depicted, indicated in (a).

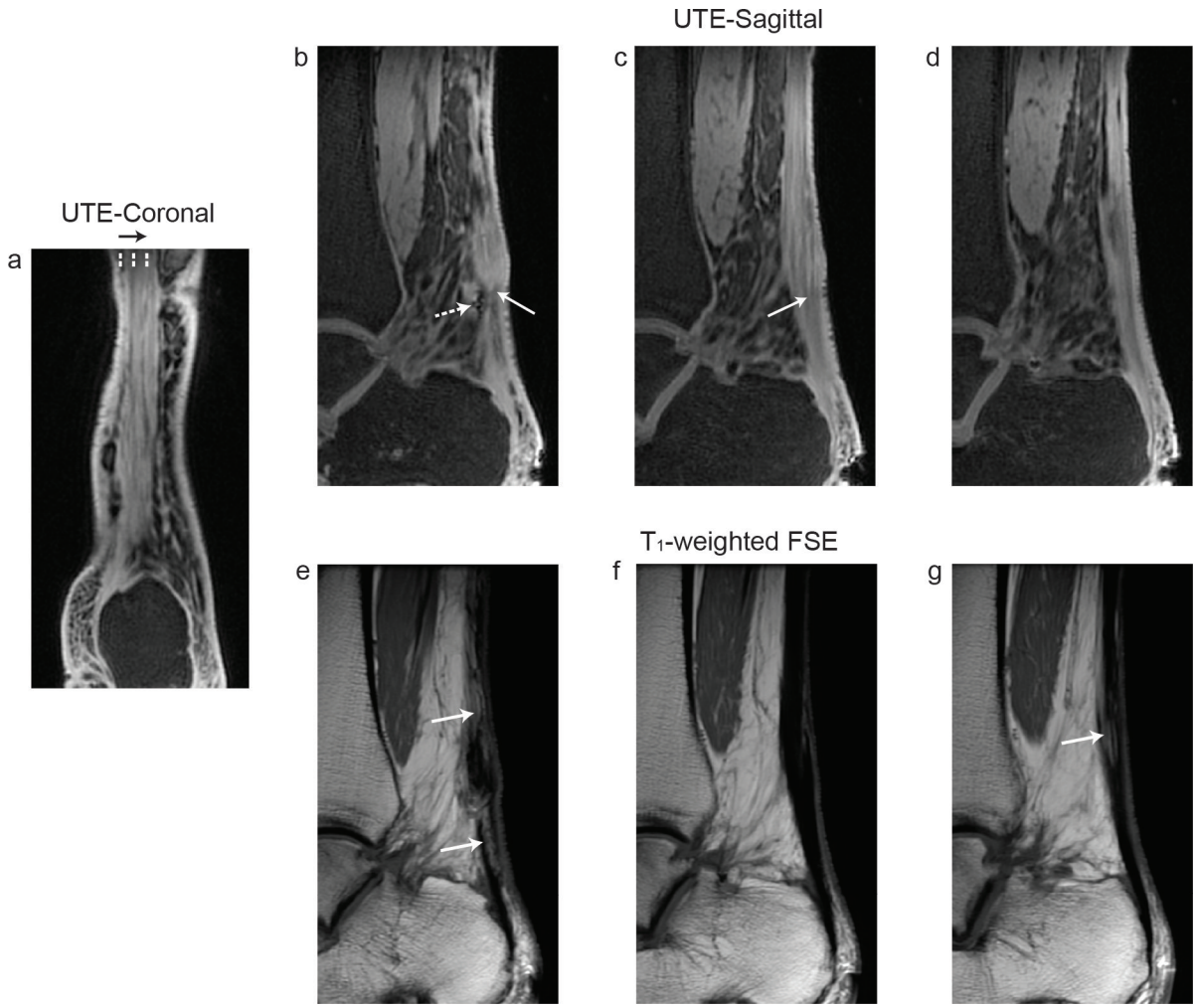

Figure 6.

Images from a 32 year old patient who underwent tendon elongation surgery right after birth. (a) UTE coronal reformatted slices. (b-d) UTE sagittal reformatted slices at three different locations denoted in (a). (e-g) T_1-weighted FSE images at the matching locations. On the FSE images, bright signal in the tendon results from fat infiltration (solid arrows). On the UTE images, disrupted microstructure and discontinuous fascicles in the region of the tendon surgical incision (solid arrows) are depicted. The yellow dotted arrow in (b) denotes susceptibility artifacts from a post surgical microscopic remnant.